

Vibro-Polaritonic IR Emission in the Strong Coupling Regime

Thibault Chervy,^{†,‡} Anoop Thomas,^{†,‡} Elias Akiki,[‡] Robrecht M. A. Vergauwe,[‡] Atef Shalabney,[§] Jino George,[‡] Eloïse Devaux,[‡] James A. Hutchison,[‡] Cyriaque Genet,[‡] and Thomas W. Ebbesen^{*,†,‡}

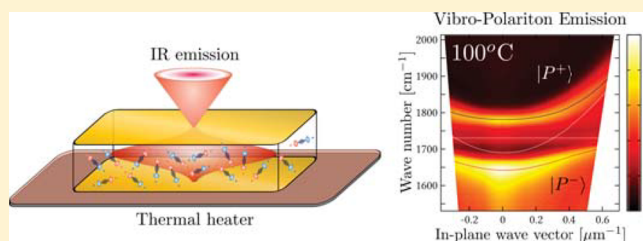
[†]University of Strasbourg, CNRS, ISIS and icFRC, 8 allée Gaspard Monge, 67000 Strasbourg, France

[§]Braude College, Snunit Street 51, Karmiel 2161002, Israel

Supporting Information

ABSTRACT: The strong coupling regime of light–matter interaction has recently been extended to IR active molecular vibrations coupled to microcavities, resulting in the formation of so-called vibro-polaritonic states. Here we demonstrate the emissivity of such hybrid states. Using thermal excitation, we achieve polaritonic IR emission from a strongly coupled polymer. Thermal excitation of vibro-polaritons, thus, constitutes an original way of establishing sizable excited-states populations in strongly coupled systems and opens new routes to the study of interacting vibro-polaritons.

KEYWORDS: vibrational strong coupling, IR emission, vibro-polariton, blackbody emission, Kirchhoff's law



1. INTRODUCTION

Some of the earliest work on light–matter strong coupling involved the theoretical study of the interaction between surface plasmon polaritons and a resonant material by Agranovich and Malshukov.¹ This inspired the first experimental demonstration of strong coupling involving a phonon mode of an inorganic salt LiF, reported in 1975.² Subsequently, strong light–matter interaction was studied with molecular excitons of J-aggregates in the early 1980s,³ as well as with inorganic semiconductors.^{4–6} In spite of the rapid development of strong coupling in inorganic semiconductors,^{7–9} it would take another 16 years before two more examples of light–molecule strong coupling were reported.^{10,11} Since then, the hybridization of molecular electronic transitions with optical resonances has attracted considerable attention, leading to many experimental achievements such as nonequilibrium Bose–Einstein condensation (BEC) of polaritons,^{12–16} superfluidity,¹⁷ enhanced conductivity,¹⁸ and new energy transfer mechanisms,^{19–21} and to much theoretical insights and progress.^{22–28} Another fascinating aspect of exciton-photon strong coupling is the possibility to achieve new material properties resulting from the formation of polaritonic states.²⁹ Following the first experimental demonstration of a modified photochemical reaction under strong coupling,³⁰ this emerging field of research is currently attracting a great interest from both theoretical^{31–37} and experimental perspectives.^{38,39}

In this context, achieving similar behaviors within the electronic ground state manifold, that is, strong coupling a vibrational transition (VSC),^{40–47} appears as a key step toward new material science and chemistry.²⁹ In particular, the first experimental demonstration of modified chemistry under VSC has recently been reported in the context of the deprotection reaction of a simple alkynylsilane,⁴⁸ and further extensions of

VSC toward biochemical systems are also being explored.⁴⁹

Coherent energy exchange and modified relaxation dynamics of vibro-polaritons has recently been demonstrated by time-resolved IR spectroscopy⁵⁰ and signatures of modified potential energy surfaces were theoretically predicted in the calculations of two-dimensional spectra.⁵¹ Moreover, polariton–polariton interaction in the vibrational ultrastrong coupling regime and the consequent appearance of polaritonic band-gaps⁵² holds promises for the observation of many-body phenomena such as BEC. In view of these recent developments, vibro-polaritonic emission is a key observable that so-far remained unexplored.

Herein, we measure the polaritonic emissivity from a typical molecular system used in the VSC regime, an organic polymer (poly(methyl methacrylate), PMMA) embedded in a metallic Fabry-Pérot (FP) cavity, resonantly tuned to one of its IR vibrational transitions. When targeting the high oscillator strength C=O stretching band of the polymer, we reach the strong coupling regime, resulting in the formation of the hybrid light–matter states $|P^+\rangle$ and $|P^-\rangle$, as schematically shown in Figure 1. By heating up the strongly coupled system, we thermally excite a population of vibro-polaritons, the radiative decay of which is directly measured using IR emission spectroscopy. Angle-resolved emission spectra are presented together with theoretical models allowing us to assess the thermalization of the vibro-polaritons.

Special Issue: Strong Coupling of Molecules to Cavities

Received: June 26, 2017

Published: October 9, 2017

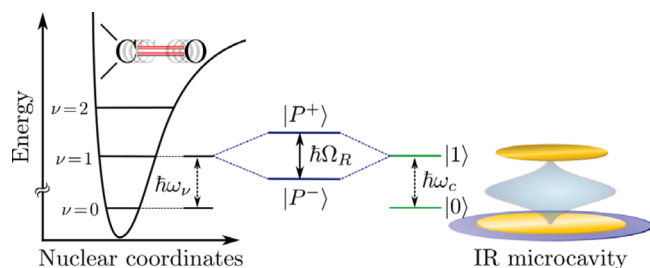


Figure 1. Energy level sketch of the strong coupling between an ensemble of identical molecular vibrational transitions (left) and the IR resonant optical mode of a Fabry-Pérot cavity (right). The collective vibro-polaritonic eigenstates of the coupled systems $|P^\pm\rangle$ are separated by the Rabi splitting $\hbar\Omega_R$, proportional to the light–matter coupling strength.

2. RESULTS AND DISCUSSION

We show in Figure 2a the IR transmission spectrum of a $2\ \mu\text{m}$ thick PMMA film spin-coated on top of a germanium (Ge) substrate. This spectrum reveals multiple sharp lines, associated

with different IR active intramolecular vibrational modes of the polymer. Superimposed on these lines, we observe a slowly varying envelope, which corresponds to FP interferences in the PMMA layer, between the air and the Ge substrate. The strong vibrational band at $1732\ \text{cm}^{-1}$ (Figure 2b blue curve, $27\ \text{cm}^{-1}$ full width at half-maximum) originates from the C=O stretching mode of the polymer backbone (see structure in Figure 2a, inset) and is the molecular resonance that we will target to achieve VSC. The black dashed curve superimposed on this spectrum is the result of transfer matrix calculation obtained by solving Maxwell’s equations for the air-Ge-PMMA-air multilayer and fitting the PMMA dielectric function to a Lorenz model with multiple resonances.^{40,52}

The IR cavity is fabricated by first sputtering a 10 nm Au mirror onto a Si wafer. A thin PMMA layer is then spin-coated on the Au mirror and baked for 1 h at $100\ ^\circ\text{C}$ to relax the strain in the polymer film and to evaporate the remaining solvent. Finally, a 10 nm layer of Au is sputtered on the film to form the FP cavity, whose modes positions are determined by the thickness of the PMMA layer. By spin-coating a $4\ \mu\text{m}$ thick

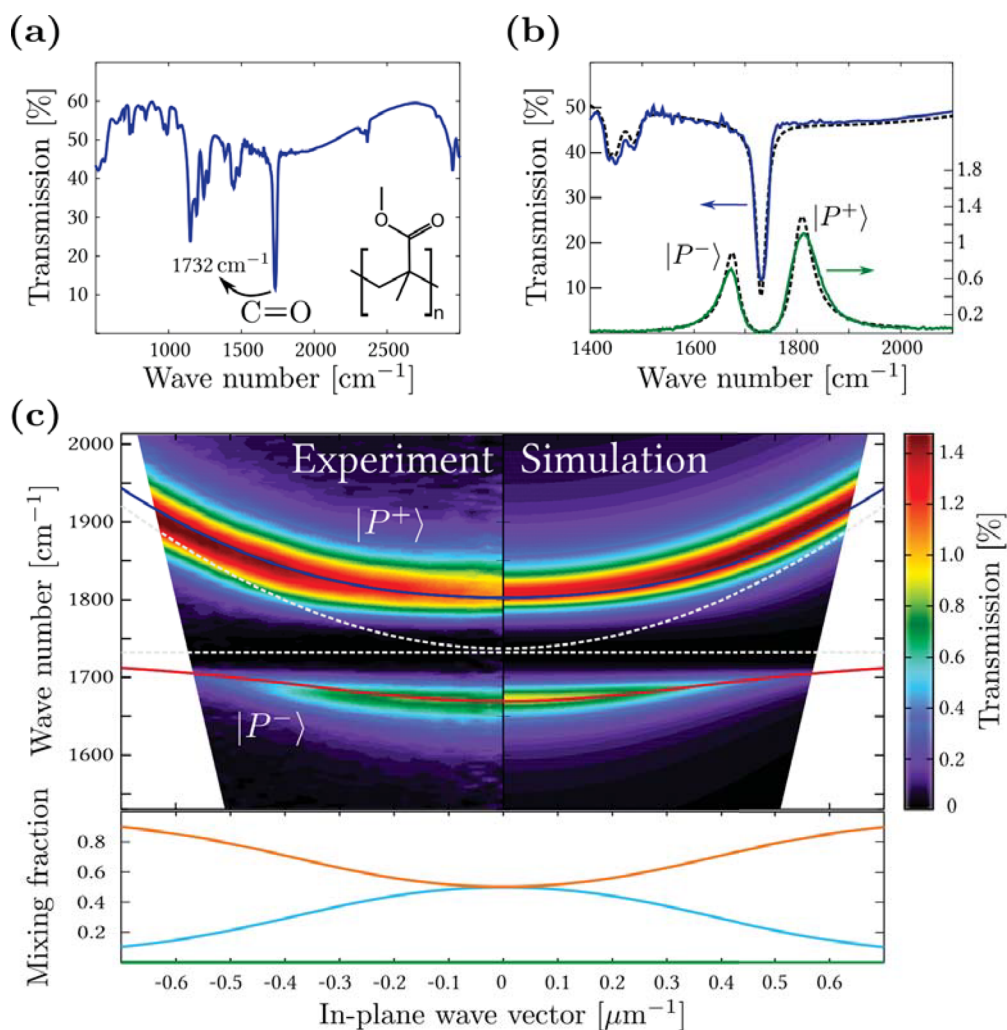


Figure 2. (a) IR transmission spectrum of a $2\ \mu\text{m}$ thick PMMA layer (molecular structure in inset) spin-coated on top of a Ge substrate. (b) IR transmission spectra of the resonantly coupled PMMA cavity (green curve), compared to the bare PMMA transmission spectrum (blue curve). The transfer matrix predictions are shown by the black dashed curves. (c) Angle-resolved transmission spectra measured under TE illumination (left) and the corresponding transfer matrix prediction (right). The solid curves are the fitted solution of the coupled oscillators model (eq 9) and the white dashed curves are the dispersions of the corresponding uncoupled modes. The lower panel shows the photonic ($|w_{\perp}|^2$, cyan curve) and the vibrational fractions ($|x_{\perp}|^2$, orange curve) composing the lower polaritonic state. The non-RWA terms $|y_{\perp}|^2$, $|z_{\perp}|^2$ are shown in green.

PMMA film, we obtain a FP cavity with a 866 cm^{-1} free spectral range (FSR), and a quality factor of about 25. The resonant coupling between the second cavity mode and the C=O stretching band of PMMA results in a cavity transmission spectrum displaying normal modes splitting of 142 cm^{-1} (Figure 2b, green curve), amounting to about 8% of the bare vibrational transition frequency and firmly placing our system in the VSC regime. This behavior is accurately reproduced by the transfer matrix calculation using the previously determined dielectric function of PMMA (dashed black curves). The slight Gaussian broadening of the experimental cavity spectrum is due to inhomogeneities in the PMMA film thickness, averaged over the region probed by the spectrometer (ca. 9 mm^2).

In order to further establish the hybrid light-matter nature of the new normal modes, we now investigate the dispersion diagram of the coupled system, using angle dependent transmission spectroscopy. As shown in Figure 2c in units of the conserved in-plane light momentum k_{\parallel} and under transverse electric (TE) polarization, the two vibro-polaritonic eigenstates undergo an avoided crossing about the vibrational C=O resonance energy (1732 cm^{-1} , white horizontal dashed line) as they disperse toward asymptotically uncoupled molecular and optical modes. The corresponding angle-dependent transfer matrix simulations, shown in the right panel of Figure 2c is again in close agreement with the measured data, albeit yielding slightly sharper modes. The expression of these new eigenstates in terms of the bare molecular and cavity modes can be derived from the following dipolar Hamiltonian, describing the coupling between a collective assembly of vibrational dipoles $\mathbf{P}(\mathbf{0}) = \sum_{i=1}^N \mathbf{p}_i$ assumed to be localized at the cavity field maximum $\mathbf{r} = \mathbf{0}$, and the electric displacement $\mathbf{D}(\mathbf{r})$ of a single m^{th} order longitudinal mode of the cavity:⁵²

$$H = H_{\text{cav}}^m + H_{\text{vib}} - \frac{1}{\epsilon_0} \mathbf{D}(\mathbf{0}) \cdot \mathbf{P}(\mathbf{0}) + \frac{1}{2\epsilon_0 V_{\nu}} \mathbf{P}(\mathbf{0})^2 \quad (1)$$

where ϵ_0 is the vacuum electric permittivity and V_{ν} corresponds to the intracavity volume occupied by the molecules. The cavity field Hamiltonian H_{cav}^m is written in terms of the position Q_c and momentum P_c quadrature operators as

$$H_{\text{cav}}^m = \frac{1}{4} \hbar \omega_c^m (Q_c^2 + P_c^2) \quad (2)$$

where the dispersive energy of the cavity mode of length L and background refractive index n writes as

$$\omega_c^m = \frac{c}{n} \sqrt{\left(\frac{m\pi}{L}\right)^2 + \|\mathbf{k}_{\parallel}\|^2} \quad (3)$$

as represented by the white dashed parabola in Figure 2c. Describing the C=O molecular stretching mode in the harmonic approximation,⁴⁰ we define the collective vibrational Hamiltonian through the vibrational position $Q_{\nu,i}$ and momentum $P_{\nu,i}$ quadratures as

$$H_{\text{vib}} = \frac{1}{4} \sum_{i=1}^N \hbar \omega_{\nu,i} (Q_{\nu,i}^2 + P_{\nu,i}^2) \quad (4)$$

where $\omega_{\nu,i}$ is the frequency of the coupled vibration. The last term in eq 1 describes the dipolar self-energy of the molecular vibrations, at the origin of the depolarization shift observed when the light-matter coupling strength approaches $\omega_{\nu,i}$.⁵³

Following the bosonization procedure detailed elsewhere,⁵² the Hamiltonian (eq 1) can be written in terms of the photonic and collective vibrational operators as

$$H = H_{\text{cav}}^m + H_{\text{vib}} - i\hbar\Omega_R (a - a^\dagger)(B + B^\dagger) + \kappa^2 (B + B^\dagger)^2 \quad (5)$$

where $a = (Q_c + iP_c)/2$ and $B = \sum_{i=1}^N (Q_{\nu,i} + iP_{\nu,i})/(2\sqrt{N})$. The collective coupling energy between the zero-point fluctuations of the field and of the vibrations, leading to the normal mode splitting writes as

$$\hbar\Omega_R = \sqrt{N} \left(\frac{\partial \langle \mathbf{p} \rangle}{\partial Q} \right)_0 \sqrt{\frac{\hbar \omega_c}{2\epsilon_0 V}} \sqrt{\frac{\hbar}{2\mu_i \omega_{\nu,i}}} \quad (6)$$

where μ_i is the oscillator reduced mass and

$$\kappa^2 = \frac{1}{2\epsilon_0 V} \left(\frac{\partial \langle \mathbf{p} \rangle}{\partial Q} \right)_0^2 \frac{\hbar}{2\mu_i \omega_{\nu,i}} \quad (7)$$

Diagonalizing this Hamiltonian through the Hopfield procedure⁵⁴ yields the vibro-polaritonic normal mode operators

$$P_{\pm} = w_{\pm} a + x_{\pm} B + y_{\pm} a^\dagger + z_{\pm} B^\dagger \quad (8)$$

associated with the eigen-energies ω_{\pm} :

$$[P_{\pm}, H] = \omega_{\pm} P_{\pm} \quad (9)$$

The resulting dispersive vibro-polaritonic energy branches are fitted to the experimental data as shown by the blue and red curves in Figure 2c, yielding a coupling strength of 133 cm^{-1} . In this fitting process, the coupling strength is the only free parameter since both the C=O vibration and the cavity mode energies can be experimentally determined independently. The squared modulus of the mixing coefficients (w, x, y, z)_±, reported in the lower panel of Figure 2c, show that the vibro-polaritonic states share a 50:50 light-vibration character at normal incidence. Moreover, for our relative coupling strength $\Omega_R/\omega_{\nu} \simeq 8\%$, the antiresonant contributions y_{\pm} and z_{\pm} usually neglected in the rotating wave approximation (RWA) remain close to zero.^{54,55}

Given this vibro-polaritonic mode structure, as revealed by IR transmission spectroscopy, we now demonstrate that the excited state polariton population in such systems can be conveniently characterized by thermal emission spectroscopy. This technique, firmly established in various research fields ranging from polymer sciences^{56,57} to mineralogy^{58,59} and astronomy,⁶⁰ has yet to be applied to the study of strongly coupled molecular systems. This holds, in part, to the fact that materials traditionally used for strong coupling are not compatible with the high temperatures needed to thermally excite a sizable population of polaritons, and one has to rely on optical or electrical excitation to study their excited states properties. In this respect, VSC of polymer films offers a unique combination of low energy vibrations and relatively high thermal resistance. For instance, the unzipping of PMMA polymer chains only occurs around a temperature of $155\text{ }^{\circ}\text{C}$.⁵⁷

The field of IR emission spectroscopy is based on the comparison between the emission L recorded from the sample of interest, and that of a blackbody L^{BB} maintained at the same temperature T . Indeed, the IR emission spectrum of a sample in thermal equilibrium is directly related to its absorption spectrum A by Kirchhoff's law:⁶¹

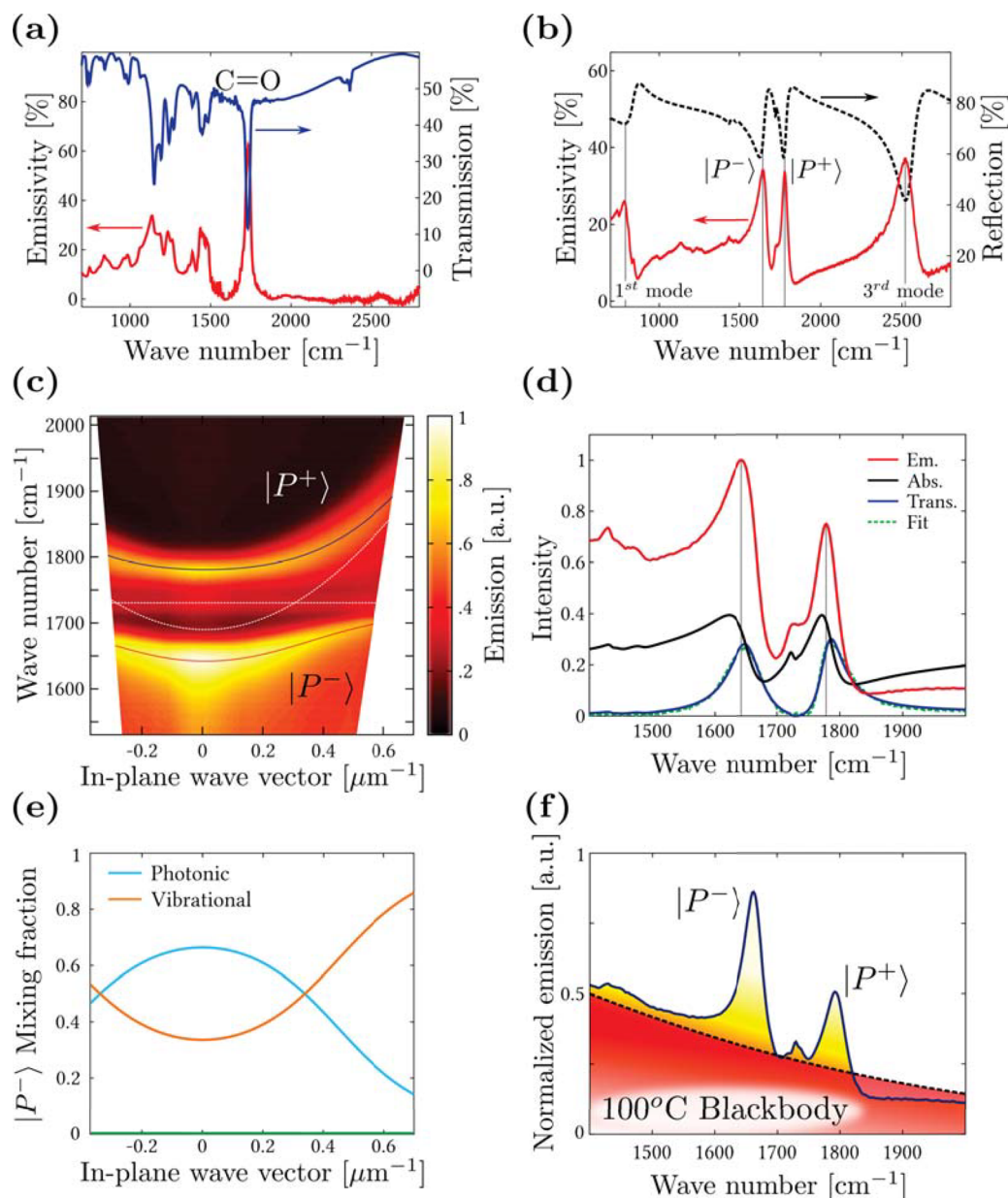


Figure 3. (a) Emissivity spectrum of a 4 μm thick film of PMMA at 100 $^{\circ}\text{C}$ (red curve). The transmission spectrum of PMMA is shown for comparison (blue curve). (b) Emissivity (red curve) and simulated cavity reflection spectrum (black dashed curve) of the strongly coupled cavity at 100 $^{\circ}\text{C}$. (c) Angle-resolved TE emission spectrum of the strongly coupled cavity corrected for the IRF and coupled-oscillator fit obtained from the previously determined parameters with a thermal expansion of 115 nm of the active layer. The corresponding Hopfield coefficients for $|P^{-}\rangle$ are shown in (e), with the photonic fraction (cyan), the vibrational fraction (orange), and the non-RWA terms (green). (d) Normal incidence spectra of the strongly coupled cavity: emission (red), absorption (black), transmission (blue), and its transfer matrix fit (green dashed curve). The transmission spectra are multiplied by 10 for clarity. The emission is corrected for the IRF. (f) Normal incidence emission-over-absorption ratio (blue curve), compared to the expected blackbody distribution at 100 $^{\circ}\text{C}$ (black dashed curve).

$$A(\nu, T) = \frac{L(\nu, T)}{L^{\text{BB}}(\nu, T)} \quad (10)$$

where ν is the spectroscopic wavenumber. This relation between IR emission and absorption allows the investigation of molecular bonds vibrations in samples for which transmission and reflection spectroscopy are not easily applicable. Examples of such samples are highly absorbing and scarcely reflecting materials, opaque and diffusing samples, and interstellar objects. Alternatively, since Kirchhoff's law is only valid for samples in thermal equilibrium, the independent determination of the IR absorption and emission allows one to

assess the thermalization of the sample under study by comparison to a blackbody emission. However, an experimentally measured blackbody emission always deviates from the ideal theoretical Planck's law due to imperfections in the instrument, thermal emission from the detector and background radiation from the heating stage and from the rest of the instrument. The deviations arising from background radiation can be accounted for by measuring the emission from a reference sample L^{ref} under the same experimental conditions. Moreover, the instrument response function (IRF) can be determined as the ratio of the measured blackbody to

the difference of the theoretical blackbody at the sample and detector temperatures:^{62,63}

$$R(\nu) = \frac{L^{\text{BB}}(\nu, T_s, T_{\text{det}})}{H_{\text{BB}}(\nu, T_s) - H_{\text{BB}}(\nu, T_{\text{det}})} \quad (11)$$

The theoretical blackbody emission is given by Planck's function

$$H_{\text{BB}}(\nu, T) = 2 \frac{hc^2\nu^3}{e^{hc\nu/k_B T} - 1} \quad (12)$$

where h and k_B are the Planck and Boltzmann constants, respectively. The difference in the denominator of eq 11 accounts for the balance in radiation flux from the sample and the detector. The emissivity spectrum of the sample ϵ is defined as

$$\epsilon = \frac{L(\nu, T) - L^{\text{ref}}(\nu, T)}{L^{\text{BB}}(\nu, T)} \quad (13)$$

where the IRF affecting each single beam measurements cancel out.

The thermal emissivity spectrum of a 4 μm thick PMMA film spin-coated onto a Si wafer and heated up to 100 $^\circ\text{C}$ is shown in Figure 3a (red curve), together with the bare PMMA IR transmission spectrum (blue curve, see the Methods section for experimental details). We clearly see in this figure that the emissivity spectrum reproduces the vibrational features observed in transmission, as expected from Kirchhoff's law in a system with a Boltzmann occupancy of excited states. This is further evidenced by comparing the emission-over-absorption ratio of the thin film to the expected Planck function. As shown in Figure S2c of the Supporting Information, this ratio can indeed be fitted by a Planck function for a temperature of 100 $^\circ\text{C}$ (black curve) at the wave numbers corresponding to vibrational transitions (nonshaded regions).⁶²

We show in Figure 3b (red curve) the normal incidence emissivity spectrum of the strongly coupled cavity, obtained by dividing the thermal emission spectrum of the cavity at 100 $^\circ\text{C}$ (Figure S1b, Supporting Information) by the blackbody emission. This spectrum shows a series of asymmetric peaks at the different cavity modes energies, as well as vibropolaritonic emission near 1700 cm^{-1} . Contrary to what has been reported in the electronic strong coupling of organic materials, where scattering results in the suppression of the $|P^+$ emission,^{64,65} we do observe comparable emissivity from both the upper and the lower vibropolaritonic states. The asymmetric line shape, although surprising at the first glance, correlates well with the simulated cavity reflection spectrum, obtained from the fit of the cavity transmission spectrum, measured at 100 $^\circ\text{C}$ (see Figure 3d). From the transfer matrix simulations, we can trace back this asymmetry to the frequency dependence of the refractive index of the Au mirrors. The thermal emissivity of the bare cavity modes is also expected from Kirchhoff's law, given the finite energy dissipation at these modes energies in the polymer and in the Au mirrors. Hence, the emission from uncoupled cavity modes can be attributed to the filtered polymer film emission, as well as to thermal emission of the Au mirrors, a contribution that could be minimized by using dielectric mirror cavities.⁴⁴

The angle-resolved TE emission spectrum of the vibropolaritons at 100 $^\circ\text{C}$, corrected for the IRF, is shown in Figures 3c and S4, together with a coupled oscillator fit. By comparing

this coupled oscillator fit to that obtained at room temperature in Figure 2c, we notice a slight thermal expansion of the intracavity layer by 115 nm, while all the other parameters of the system remain unchanged. Contrary to the emissivity data presented in Figure 3a,b, the emission dispersion diagram of panel (c) is not divided by a blackbody spectrum, thus, allowing the observation of the actual vibropolaritons populations. Dispersive contributions from both the upper and lower vibropolaritons are clearly identified, with a stronger emission coming from the bottom of the $|P^- \rangle$ branch. Such an intensity distribution is very suggestive of an interaction-mediated polariton relaxation mechanism, akin to those required for polariton condensation in other strongly coupled systems.^{12,66} Alternatively, it could be related to the angle-dependent photonic and vibrational mixture composing the polaritonic states⁶⁷ (see Figure 3e). As shown in Figure S5 of the Supporting Information, cavities of various detunings, yielding different photonic and vibrational contents of the polaritons, all display the same qualitative behavior with a higher emission intensity from the bottom of the $|P^- \rangle$ branch. These observations point toward the absence of a relaxation bottleneck for vibropolaritons, as opposed to what has been reported in the context of electronic strong coupling.^{68,69} Further experiments are however needed to address this point, a detailed study of the temperature and detuning dependence of vibropolariton emission being beyond the scope of this paper.

Interestingly, a close examination of the spectra of Figure 3b reveals that the polaritons emissivity peaks are blue-shifted with respect to the corresponding reflectivity dips. This offset, amounting to 17 cm^{-1} for $|P^- \rangle$ and 6 cm^{-1} for $|P^+ \rangle$, is absent for the uncoupled 1st and 3rd cavity modes (see also Figure S5a of the Supporting Information). This behavior is clearly displayed in Figure 3d, where we compare the emission spectrum of the polariton to their transmission and absorption spectra. Surprisingly, the polariton emission peaks lie in between the transmission and the absorption maxima, in striking contrast to what would be expected from Kirchhoff's law. This nonthermalized population distribution of vibropolaritons is further evidenced by comparing their normalized emission-over-absorption spectrum to the theoretical blackbody distribution. While Kirchhoff's law holds for the nonzero background emission of the system, it clearly fails near the vibropolaritons energies (Figure 3f). As displayed in Figure S5b of the Supporting Information, the nonthermalized part of the polariton emission is more pronounced on the high energy side of the polaritonic modes, an important information for a detailed microscopic model of polariton-polariton interactions. Indeed, the origin of the blue-shifted vibropolariton emission is probably due to polariton-polariton interactions as already observed in inorganic systems.^{70,71} We further verify in Figure S2 of the Supporting Information that both the bare PMMA film and the empty FP cavity modes do satisfy Kirchhoff's law, ruling out the possibility that the reported polariton emission originates from a simple optical filter effect. Thus, the observation of nonthermalized emission from the strongly coupled cavity constitutes a direct proof of genuine polaritonic signatures in the IR emission spectrum. Conversely, it illustrates how strong coupling a thermalized emitter to a structured electromagnetic field can result in polaritonic states with modified relaxation pathways and dynamics.

In summary, we have demonstrated the emissivity of vibropolaritonic states in a strongly coupled polymer microcavity. By

Table 1. Parameters Obtained from the Fit of the Transmission Spectrum of the Bare PMMA film on Ge^a

ϵ_b	f_1	k_{01}	Γ_1	f_2	k_{02}	Γ_2	f_3	k_{03}	Γ_3	f_4	k_{04}	Γ_4
1.8	3.26	1.73	1.54	0.40	1.48	25	0.60	1.45	25	0.15	1.44	10

^aAll oscillator strengths f_j are in 10^4 cm^{-2} . The resonant wave vectors k_{0j} are in 10^3 cm^{-1} . The phenomenological damping constants Γ_j are in cm^{-1} .

thermally promoting a broadband population of vibro-polaritons, we characterized their emissivity spectra and momentum distributions. Our results show that the polaritonic emission is not thermalized. This observation points toward vibro-polariton interactions leading to nonthermalized state occupancy and lays the ground for the investigation of vibro-polariton condensation. This study establishes polariton IR emission spectroscopy as a complementary approach to recent experiments on time-resolved dynamics,⁵⁰ opening the possibility to investigate energy transfer processes in the vibrational strong coupling regime.

3. METHODS

3.1. Sample Preparation. To prepare the active layer, a concentrated solution of PMMA (16 wt %) was first prepared in trichloro ethylene. Both PMMA ($M_w = 996000$) and trichloroethylene were purchased from Sigma-Aldrich and used without any further purification. The solution was then spin-coated at a high speed (ca. 5000 rpm) to form a 4 μm thick film.

3.2. FTIR Emission Spectroscopy. The measurements were performed on a Bruker FTIR Vertex 70 spectrometer, by keeping the sample of interest in the side input port. Emission spectra were recorded using a liquid nitrogen cooled mercury–cadmium–telluride detector, with a resolution of 4 cm^{-1} . The sample was mounted on a computer-controlled rotating stage and heated from the back by a Peltier stage. The surface temperature of the sample was kept constant throughout the study and was continuously monitored by a thermocouple. The cavity emission spectra were referenced to that of a 20 nm Au-coated Si wafer, measured at the same angles. The bare film emission spectra were referenced to that of a bare Si wafer. Emissivity data were obtained by normalizing these referenced spectra to the emission of a homemade blackbody sample, obtained by coating a Si wafer with a thick layer of carbon soot. Each single beam measurements were normalized by the instrument response function (IRF). The IRF $R(\nu)$, determined as the ratio of the emission of carbon soot to the balanced Planck distributions of the sample and the detector, see eq 11, is shown in Figure S1(a), black curve.

3.3. Transfer Matrix Simulations. The fit of transfer matrix simulation to the bare PMMA film transmission spectrum was obtained using the following multi-Lorentzian dielectric function for PMMA:

$$\epsilon(k) = \epsilon_B - \sum_{j=1}^N \frac{f_j}{k^2 - k_j^2 + ik\Gamma_j} \quad (14)$$

where ϵ_B is the background dielectric function of the medium and f_j , k_j , and Γ_j are, respectively, the oscillator strength, the resonant wavenumber, and the damping constant of the vibrational band j . The best fit was achieved for the set of parameters given in Table 1. This dielectric function was further used to simulate the strongly coupled cavity spectra. The refractive indices of Ge and Si were obtained from the literature,⁷² and the thin Au mirror refractive index was

obtained from a modified Lorenz-Drude equation as described elsewhere.⁴⁰

■ ASSOCIATED CONTENT

📄 Supporting Information

The Supporting Information is available free of charge on the ACS Publications website at DOI: 10.1021/acsp Photonics.7b00677.

Single beam emission spectra; Absorption, emission and normalized emission spectra for the bare PMMA film and the empty FP cavity; Angle dependent cavity emission spectra; Dispersion diagrams and angle resolved emission spectra for detuned cavities at 75 °C and 100 °C; Comparison of emissivity, reflection, emission and emission-overabsorption spectra; Round-trip phase accumulation calculation (PDF).

■ AUTHOR INFORMATION

Corresponding Author

*E-mail: ebbesen@unistra.fr.

ORCID

Thomas W. Ebbesen: 0000-0002-3999-1636

Author Contributions

†T.C. and A.T. contributed equally to this work.

Notes

The authors declare no competing financial interest.

■ ACKNOWLEDGMENTS

We acknowledge support of the International Center for Frontier Research in Chemistry (icFRC, Strasbourg), the ANR Equipex Union (ANR-10-EQPX-52-01), the Labex NIE Projects (ANR-11-LABX-0058 NIE), and CSC (ANR-10-LABX-0026 CSC) within the Investissement d'Avenir program ANR-10-IDEX-0002-02.

■ REFERENCES

- (1) Agranovich, V.; Malshukov, A. Surface polariton spectra if the resonance with the transition layer vibrations exist. *Opt. Commun.* **1974**, *11*, 169–171.
- (2) Yakovlev, V.; Nazin, V.; Zhizhin, G. The surface polariton splitting due to thin surface film LO vibrations. *Opt. Commun.* **1975**, *15*, 293–295.
- (3) Pockrand, I.; Brillante, A.; Möbius, D. Exciton-surface plasmon coupling: An experimental investigation. *J. Chem. Phys.* **1982**, *77*, 6289–6295.
- (4) Weisbuch, C.; Nishioka, M.; Ishikawa, A.; Arakawa, Y. Observation of the coupled exciton-photon mode splitting in a semiconductor quantum microcavity. *Phys. Rev. Lett.* **1992**, *69*, 3314–3317.
- (5) Houdré, R.; Weisbuch, C.; Stanley, R. P.; Oesterle, U.; Pellandini, P.; Ilegems, M. Measurement of Cavity-Polariton Dispersion Curve from Angle-Resolved Photoluminescence Experiments. *Phys. Rev. Lett.* **1994**, *73*, 2043–2046.
- (6) Norris, T. B.; Rhee, J.-K.; Sung, C.-Y.; Arakawa, Y.; Nishioka, M.; Weisbuch, C. Time-resolved vacuum Rabi oscillations in a semiconductor quantum microcavity. *Phys. Rev. B: Condens. Matter Mater. Phys.* **1994**, *50*, 14663–14666.

- (7) Skolnick, M. S.; Fisher, T. A.; Whittaker, D. M. Strong coupling phenomena in quantum microcavity structures. *Semicond. Sci. Technol.* **1998**, *13*, 645.
- (8) Houdré, R. Early stages of continuous wave experiments on cavity-polaritons. *Phys. Status Solidi B* **2005**, *242*, 2167–2196.
- (9) Deng, H.; Haug, H.; Yamamoto, Y. Exciton-polariton Bose–Einstein condensation. *Rev. Mod. Phys.* **2010**, *82*, 1489–1537.
- (10) Fujita, T.; Sato, Y.; Kuitani, T.; Ishihara, T. Tunable polariton absorption of distributed feedback microcavities at room temperature. *Phys. Rev. B: Condens. Matter Mater. Phys.* **1998**, *57*, 12428–12434.
- (11) Lidzey, D. G.; Bradley, D. D. C.; Skolnick, M. S.; Virgili, T.; Walker, S.; Whittaker, D. M. Strong exciton-photon coupling in an organic semiconductor microcavity. *Nature* **1998**, *395*, 53–55.
- (12) Kéna-Cohen, S.; Forrest, S. Room-temperature polariton lasing in an organic single-crystal microcavity. *Nat. Photonics* **2010**, *4*, 371–375.
- (13) Plumhof, J. D.; Stöferle, T.; Mai, L.; Scherf, U.; Mahrt, R. F. Room-temperature Bose–Einstein condensation of cavity exciton-polaritons in a polymer. *Nat. Mater.* **2013**, *13*, 247–252.
- (14) Daskalakis, K.; Maier, S.; Murray, R.; Kéna-Cohen, S. Nonlinear interactions in an organic polariton condensate. *Nat. Mater.* **2014**, *13*, 271–278.
- (15) Dietrich, C. P.; Steude, A.; Tropf, L.; Schubert, M.; Kronenberg, N. M.; Ostermann, K.; Höfiling, S.; Gather, M. C. An exciton-polariton laser based on biologically produced fluorescent protein. *Sci. Adv.* **2016**, *2*, e1600666.
- (16) Ramezani, M.; Halpin, A.; Fernández-Domínguez, A. I.; Feist, J.; Rodríguez, S. R.-K.; Garcia-Vidal, F. J.; Rivas, J. G. Plasmon-exciton-polariton lasing. *Optica* **2017**, *4*, 31–37.
- (17) Lerario, G.; Fieramosca, A.; Barachati, F.; Ballarini, D.; Daskalakis, K. S.; Dominici, L.; De Giorgi, M.; Maier, S. A.; Gigli, G.; Kéna-Cohen, S.; Sanvitto, D. Room-temperature superfluidity in a polariton condensate. *Nat. Phys.* **2017**, *13*, 837–841.
- (18) Orgiu, E.; George, J.; Hutchison, J. A.; Devaux, E.; Dayen, J. F.; Doudin, B.; Stellacci, F.; Genet, C.; Schachenmayer, J.; Genes, C.; Pupillo, G.; Samori, P.; Ebbesen, T. W. Conductivity in organic semiconductors hybridized with the vacuum field. *Nat. Mater.* **2015**, *14*, 1123–1129.
- (19) Coles, D. M.; Somaschi, N.; Michetti, P.; Clark, C.; Lagoudakis, P. G.; Savvidis, P. G.; Lidzey, D. G. Polariton-mediated energy transfer between organic dyes in a strongly coupled optical microcavity. *Nat. Mater.* **2014**, *13*, 712–719.
- (20) Zhong, X.; Chervy, T.; Wang, S.; George, J.; Thomas, A.; Hutchison, J. A.; Devaux, E.; Genet, C.; Ebbesen, T. W. Non-Radiative Energy Transfer Mediated by Hybrid Light-Matter States. *Angew. Chem., Int. Ed.* **2016**, *55*, 6202–6206.
- (21) Zhong, X.; Chervy, T.; Zhang, L.; Thomas, A.; George, J.; Genet, C.; Hutchison, J.; Ebbesen, T. W. Energy Transfer between Spatially Separated Entangled Molecules. *Angew. Chem., Int. Ed.* **2017**, *56*, 9034–9038.
- (22) Agranovich, V. M.; Litniskaia, M.; Lidzey, D. G. Cavity polaritons in microcavities containing disordered organic semiconductors. *Phys. Rev. B: Condens. Matter Mater. Phys.* **2003**, *67*, 085311.
- (23) Michetti, P.; La Rocca, G. C. Polariton states in disordered organic microcavities. *Phys. Rev. B: Condens. Matter Mater. Phys.* **2005**, *71*, 115320.
- (24) Mazza, L.; Fontanesi, L.; La Rocca, G. C. Organic-based microcavities with vibronic progressions: Photoluminescence. *Phys. Rev. B: Condens. Matter Mater. Phys.* **2009**, *80*, 235314.
- (25) González-Tudela, A.; Huidobro, P. A.; Martín-Moreno, L.; Tejedor, C.; García-Vidal, F. J. Theory of Strong Coupling between Quantum Emitters and Propagating Surface Plasmons. *Phys. Rev. Lett.* **2013**, *110*, 126801.
- (26) Feist, J.; Garcia-Vidal, F. J. Extraordinary Exciton Conductance Induced by Strong Coupling. *Phys. Rev. Lett.* **2015**, *114*, 196402.
- (27) Schachenmayer, J.; Genes, C.; Tignone, E.; Pupillo, G. Cavity-Enhanced Transport of Excitons. *Phys. Rev. Lett.* **2015**, *114*, 196403.
- (28) Hagenmüller, D.; Schachenmayer, J.; Schütz, S.; Genes, C.; Pupillo, G. Cavity-enhanced transport of charge. *arXiv preprint arXiv:1703.00803* **2017**.
- (29) Ebbesen, T. W. Hybrid Light-Matter States in a Molecular and Material Science Perspective. *Acc. Chem. Res.* **2016**, *49*, 2403–2412.
- (30) Hutchison, J. A.; Schwartz, T.; Genet, C.; Devaux, E.; Ebbesen, T. W. Modifying Chemical Landscapes by Coupling to Vacuum Fields. *Angew. Chem., Int. Ed.* **2012**, *51*, 1592–1596.
- (31) Spano, F. C. Optical microcavities enhance the exciton coherence length and eliminate vibronic coupling in J-aggregates. *J. Chem. Phys.* **2015**, *142*, 184707.
- (32) Canaguier-Durand, A.; Genet, C.; Lambrecht, A.; Ebbesen, T. W.; Reynaud, S. Non-Markovian polariton dynamics in organic strong coupling. *Eur. Phys. J. D* **2015**, *69*, 24.
- (33) Galego, J.; Garcia-Vidal, F. J.; Feist, J. Suppressing photochemical reactions with quantized light fields. *Nat. Commun.* **2016**, *7*, 13841.
- (34) Wu, N.; Feist, J.; Garcia-Vidal, F. J. When polarons meet polaritons: Exciton-vibration interactions in organic molecules strongly coupled to confined light fields. *Phys. Rev. B: Condens. Matter Mater. Phys.* **2016**, *94*, 195409.
- (35) Kowalewski, M.; Bennett, K.; Mukamel, S. Cavity Femtochemistry: Manipulating Nonadiabatic Dynamics at Avoided Crossings. *J. Phys. Chem. Lett.* **2016**, *7*, 2050–2054.
- (36) Herrera, F.; Spano, F. C. Cavity-Controlled Chemistry in Molecular Ensembles. *Phys. Rev. Lett.* **2016**, *116*, 238301.
- (37) Flick, J.; Ruggenthaler, M.; Appel, H.; Rubio, A. Atoms and molecules in cavities, from weak to strong coupling in quantum-electrodynamics (QED) chemistry. *Proc. Natl. Acad. Sci. U. S. A.* **2017**, *114*, 3026–3034.
- (38) Hutchison, J. A.; Liscio, A.; Schwartz, T.; Canaguier-Durand, A.; Genet, C.; Palermo, V.; Samori, P.; Ebbesen, T. W. Tuning the Work-Function Via Strong Coupling. *Adv. Mater.* **2013**, *25*, 2481–2485.
- (39) Wang, S.; Mika, A.; Hutchison, J. A.; Genet, C.; Jouaiti, A.; Hosseini, M. W.; Ebbesen, T. W. Phase transition of a perovskite strongly coupled to the vacuum field. *Nanoscale* **2014**, *6*, 7243–7248.
- (40) Shalabney, A.; George, J.; Hutchison, J.; Pupillo, G.; Genet, C.; Ebbesen, T. W. Coherent coupling of molecular resonators with a microcavity mode. *Nat. Commun.* **2015**, *6*, 5981.
- (41) Long, J. P.; Simpkins, B. S. Coherent Coupling between a Molecular Vibration and Fabry-Pérot Optical Cavity to Give Hybridized States in the Strong Coupling Limit. *ACS Photonics* **2015**, *2*, 130–136.
- (42) George, J.; Shalabney, A.; Hutchison, J. A.; Genet, C.; Ebbesen, T. W. Liquid-Phase Vibrational Strong Coupling. *J. Phys. Chem. Lett.* **2015**, *6*, 1027–1031.
- (43) Simpkins, B. S.; Fears, K. P.; Dressick, W. J.; Spann, B. T.; Dunkelberger, A. D.; Owrutsky, J. C. Spanning Strong to Weak Normal Mode Coupling between Vibrational and Fabry-Pérot Cavity Modes through Tuning of Vibrational Absorption Strength. *ACS Photonics* **2015**, *2*, 1460–1467.
- (44) Muallem, M.; Palatnik, A.; Nessim, G. D.; Tischler, Y. R. Strong light-matter coupling between a molecular vibrational mode in a PMMA film and a low-loss mid-IR microcavity. *Ann. Phys.* **2016**, *528*, 313–320.
- (45) Casey, S. R.; Sparks, J. R. Vibrational Strong Coupling of Organometallic Complexes. *J. Phys. Chem. C* **2016**, *120*, 28138–28143.
- (46) Memmi, H.; Benson, O.; Sadofev, S.; Kalusniak, S. Strong Coupling between Surface Plasmon Polaritons and Molecular Vibrations. *Phys. Rev. Lett.* **2017**, *118*, 126802.
- (47) del Pino, J.; Feist, J.; Garcia-Vidal, F. J. Quantum theory of collective strong coupling of molecular vibrations with a microcavity mode. *New J. Phys.* **2015**, *17*, 053040.
- (48) Thomas, A.; George, J.; Shalabney, A.; Dryzhakov, M.; Varma, S. J.; Moran, J.; Chervy, T.; Zhong, X.; Devaux, E.; Genet, C.; Hutchison, J. A.; Ebbesen, T. W. Ground-State Chemical Reactivity under Vibrational Coupling to the Vacuum Electromagnetic Field. *Angew. Chem., Int. Ed.* **2016**, *55*, 11462–11466.

- (49) Vergauwe, R. M. A.; George, J.; Chervy, T.; Hutchison, J. A.; Shalabney, A.; Torbeev, V. Y.; Ebbesen, T. W. Quantum Strong Coupling with Protein Vibrational Modes. *J. Phys. Chem. Lett.* **2016**, *7*, 4159–4164.
- (50) Dunkelberger, A.; Spann, B.; Fears, K.; Simpkins, B.; Owrutsky, J. Modified relaxation dynamics and coherent energy exchange in coupled vibration-cavity polaritons. *Nat. Commun.* **2016**, *7*, 13504.
- (51) Saurabh, P.; Mukamel, S. Two-dimensional infrared spectroscopy of vibrational polaritons of molecules in an optical cavity. *J. Chem. Phys.* **2016**, *144*, 124115.
- (52) George, J.; Chervy, T.; Shalabney, A.; Devaux, E.; Hiura, H.; Genet, C.; Ebbesen, T. W. Multiple Rabi Splittings under Ultrastrong Vibrational Coupling. *Phys. Rev. Lett.* **2016**, *117*, 153601.
- (53) Todorov, Y.; Andrews, A. M.; Colombelli, R.; De Liberato, S.; Ciuti, C.; Klang, P.; Strasser, G.; Sirtori, C. Ultrastrong light-matter coupling regime with polariton dots. *Phys. Rev. Lett.* **2010**, *105*, 196402.
- (54) Hopfield, J. Theory of the contribution of excitons to the complex dielectric constant of crystals. *Phys. Rev.* **1958**, *112*, 1555.
- (55) Ciuti, C.; Bastard, G.; Carusotto, I. Quantum vacuum properties of the intersubband cavity polariton field. *Phys. Rev. B: Condens. Matter Mater. Phys.* **2005**, *72*, 115303.
- (56) Bernath, P. F. Infrared emission spectroscopy. *Annu. Rep. Prog. Chem., Sect. C: Phys. Chem.* **2000**, *96*, 177–224.
- (57) Celina, M.; Ottesen, D.; Gillen, K.; Clough, R. FTIR emission spectroscopy applied to polymer degradation. *Polym. Degrad. Stab.* **1997**, *58*, 15–31.
- (58) Ruff, S. W.; Christensen, P. R.; Barbera, P. W.; Anderson, D. L. Quantitative thermal emission spectroscopy of minerals: A laboratory technique for measurement and calibration. *J. Geophys. Res.* **1997**, *102*, 14899–14913.
- (59) Christensen, P. R.; et al. Miniature Thermal Emission Spectrometer for the Mars Exploration Rovers. *J. Geophys. Res.* **2003**, *108*, 8064.
- (60) Léger, A.; d'Hendecourt, L.; Defourneau, D. Physics of IR emission by interstellar PAH molecules. *Astron. Astrophys.* **1989**, *216*, 148–164.
- (61) Salisbury, J. W.; Wald, A.; D'Aria, D. M. Thermal-infrared remote sensing and Kirchhoff's law: 1. Laboratory measurements. *J. Geophys. Res.* **1994**, *99*, 11897–11911.
- (62) Solomon, P. R.; Best, P. E.; Carangelo, R. M.; Markham, J. R.; Chien, P.-L.; Santoro, R. J.; Semerjian, H. G. FT-IR emission/transmission spectroscopy for in situ combustion diagnostics. *Symp. (Int.) Combust., [Proc.]* **1988**, *21*, 1763–1771.
- (63) Mink, J. *Handbook of Vibrational Spectroscopy*; John Wiley & Sons, Ltd, 2006.
- (64) Coles, D. M.; Michetti, P.; Clark, C.; Tsoi, W. C.; Adawi, A. M.; Kim, J.-S.; Lidzey, D. G. Vibrationally Assisted Polariton-Relaxation Processes in Strongly Coupled Organic-Semiconductor Microcavities. *Adv. Funct. Mater.* **2011**, *21*, 3691–3696.
- (65) George, J.; Wang, S.; Chervy, T.; Canaguier-Durand, A.; Schaeffer, G.; Lehn, J.-M.; Hutchison, J. A.; Genet, C.; Ebbesen, T. W. Ultra-strong coupling of molecular materials: spectroscopy and dynamics. *Faraday Discuss.* **2015**, *178*, 281–294.
- (66) Corfdir, P.; Levrat, J.; Rossbach, G.; Butté, R.; Feltin, E.; Carlin, J.-F.; Christmann, G.; Lefebvre, P.; Ganière, J.-D.; Grandjean, N.; Deveaud-Plédran, B. Impact of biexcitons on the relaxation mechanisms of polaritons in III-nitride based multiple quantum well microcavities. *Phys. Rev. B: Condens. Matter Mater. Phys.* **2012**, *85*, 245308.
- (67) Coles, D. M.; Grant, R. T.; Lidzey, D. G.; Clark, C.; Lagoudakis, P. G. Imaging the polariton relaxation bottleneck in strongly coupled organic semiconductor microcavities. *Phys. Rev. B: Condens. Matter Mater. Phys.* **2013**, *88*, 121303.
- (68) Tassone, F.; Piermarocchi, C.; Savona, V.; Quattropani, A.; Schwendimann, P. Bottleneck effects in the relaxation and photoluminescence of microcavity polaritons. *Phys. Rev. B: Condens. Matter Mater. Phys.* **1997**, *56*, 7554–7563.
- (69) Tartakovskii, A. I.; Emam-Ismael, M.; Stevenson, R. M.; Skolnick, M. S.; Astratov, V. N.; Whittaker, D. M.; Baumberg, J. J.; Roberts, J. S. Relaxation bottleneck and its suppression in semiconductor microcavities. *Phys. Rev. B: Condens. Matter Mater. Phys.* **2000**, *62*, R2283–R2286.
- (70) Savvidis, P. G.; Baumberg, J. J.; Stevenson, R. M.; Skolnick, M. S.; Whittaker, D. M.; Roberts, J. S. Angle-Resonant Stimulated Polariton Amplifier. *Phys. Rev. Lett.* **2000**, *84*, 1547–1550.
- (71) Ciuti, C.; Schwendimann, P.; Deveaud, B.; Quattropani, A. Theory of the angle-resonant polariton amplifier. *Phys. Rev. B: Condens. Matter Mater. Phys.* **2000**, *62*, R4825–R4828.
- (72) Aspnes, D. E.; Studna, A. A. Dielectric functions and optical parameters of Si, Ge, GaP, GaAs, GaSb, InP, InAs, and InSb from 1.5 to 6.0 eV. *Phys. Rev. B: Condens. Matter Mater. Phys.* **1983**, *27*, 985–1009.